Available online at www.sciencedirect.com

ScienceDirect

Energy Procedia 101 (2016) 734 – 741

Energy Procedia

71st Conference of the Italian Thermal Machines Engineering Association, ATI2016, 14-16 September 2016, Turin, Italy

Estimation of the Aerodynamic Force Induced by Vaneless Diffuser Rotating Stall in Centrifugal Compressor Stages

Michele Marconcini[a], Alessandro Bianchini[a], Matteo Checcucci[a], Davide Biliotti[b], Marco Giachi[b], Dante Tommaso Rubino[b], Andrea Arnone[a], Lorenzo Ferrari[c]*, Giovanni Ferrara[a]

[a]*Department of Industrial Engineering, Università degli Studi di Firenze, Via di Santa Marta 3, 50139 Firenze, Italy*
[b]*GE Oil&Gas, Via Felice Matteucci 10, 50127 Firenze, Italy*
[c]*CNR-ICCOM, Consiglio Nazionale delle Ricerche, Via Madonna del Piano 10, 50019 Sesto Fiorentino, Italy*

Abstract

Rotating stall in centrifugal compressors not only adversely affects the performance before surge, but also can generate high subsynchronous vibrations, marking the minimum flow limit of a machine. Recent works presented an experimental approach to estimate the stall force induced by the unbalanced pressure field in a vaneless diffuser using dynamic pressure measurements. In this study, the results of a 3D-unsteady simulation of a radial stage model were used to estimate the stall force and to compare it with the approximation obtained with an "experimental-like" approach. Results showed that: *a)* the experimental approach, using an ensemble average approach for transposing data between time and space domains provides sufficiently accurate results; *b)* the momentum contribution, neglected in experiments, gives negligible contribution to the final intensity of the stall force.

Peer-review under responsibility of the Scientific Committee of ATI 2016.

Keywords: centrifugal compressor; CFD; rotating stall; experimental analysis; stall force

1. Introduction

Centrifugal compressors play a fundamental role in the present world energy scenario, particularly for oil & gas industries [1]. Due to the huge amount of power associated to their industrial applications, even small efficiency

* Corresponding author. Tel.: +39-055-275-8797; fax: +39-055-275-8755.
E-mail address: lorenzo.ferrari@iccom.cnr.it

Peer-review under responsibility of the Scientific Committee of ATI 2016.
doi:10.1016/j.egypro.2016.11.093

and/or rangeability increases would in fact provide significant energy and money savings. In view of an extension of the minimum flow limit, in particular, manufacturers pay much interest to an inner comprehension of the aerodynamic phenomena which precede the surge, with particular focus on rotating stall (e.g. [2-9]). Recent studies in fact showed that a proper estimation of the aerodynamic forces generated during rotating stall conditions [10], and a consequent revised design of the stages [11], could provide notable increases of expected rangeability.

Nomenclature

b	diffuser width	[m]
f	mass forces	[N]
F	force	[N]
n	versor normal to surface	
p	pressure	[Pa]
S	surface of the control volume	
t	time	[s]
T	revolution period	[s]
u	flow velocity	[m/s]
V	control volume	
y^+	dimensionless wall distance	[-]
Greek letters		
θ	azimuthal angle	[deg]
ρ	air density	[kg/Nm^3]
τ	work coefficient	[-]
τ_w	viscous stresses	[N]
ϕ	flow coefficient	[-]
ω	pulsation	[rad/s]
Superscripts		
*	dimensionless value	
Subscripts		
e	external	
m	momentum	
p	pressure	
r	radial	
stall	value at stall	

1.1. Experimental approach to stall force estimation

The evaluation of the destabilizing force generated by the unbalanced flow field during rotating stall is not easy in real compressors, since the use of laboratory-like measurement system is very often not allowed by mechanical constraints or reliability issues. Some of the authors have assessed in the last few years a systematic approach for determining the stall force in vaneless diffuser rotating stall making use of a limited number of dynamic pressure sensors positioned at the diffuser's inlet [10,12]. The approach is based on at least two sensors inserted at given azimuthal positions within the diffuser, whose signals in time are manipulated with an ensemble average approach clocked at the subsynchronous revolution frequency of the stall. This frequency is identified by the autocorrelation function of one of the signals, while the cross-correlation function is used to define the phase shift between the signals at that frequency and then calculate the number of lobes of the stall pattern, cross-checking the proper selection of the stall frequency [10,12]. The method has been validated against experimental data [10-11], obtaining a satisfactory agreement. As discussed by the authors themselves, however, some important assumptions are needed in applying the methodology. First, the pressure pattern induced by the stall is assumed to be stable during its rotation [13]; by doing so, pressure data acquired can be transposed from the time domain to the space domain.

Then, the effect of induced distortions of the radial velocity distribution at the impeller exit (i.e. the non-uniformity of momentum distribution) is assumed to be small enough with respect to the pressure contribution to be neglected in a first approximation. Finally, the instantaneous force pulsations due to all phenomena taking place at frequencies higher than the stall one are smoothed by the ensemble average process on many cycles, leading to the estimation of a constant stall force intensity [12].

1.2. Theoretical analysis

From a theoretical point of view, the mathematical expression of the force on the impeller can be easily obtained applying the momentum balance (Eq. 1) to a control volume containing the impeller, schematized in Fig.1(a). By applying the transport theorem to the le left term of Eq. 1, the balance can then be expressed as in Eq. 2, where F_e represents the sum of all forces acting on the control volume surface. Finally, if one neglects the body forces (first element of the right term in Eq. 2), the resulting force on the impeller (F) is given by Eq. 3, where the pressure and momentum in the inlet (S_1) and outlet (S_2) surfaces contributions are clearly distinguishable. It is worth remembering that the same force could be also expressed as the integral of viscous and pressure stresses acting on the lateral boundaries of the control volume S, representing the walls of the impeller.

$$\frac{d}{dt}\int_V \rho \underline{u} dV = \int_V \rho \underline{f} dV + \int_S \underline{F} dS \tag{1}$$

$$\frac{\partial}{\partial t}\int_V \rho \underline{u} dV + \int_S \rho \underline{u}(\underline{u}\cdot\underline{n}) dS = \int_V \rho \underline{f} dV + \int_S \underline{F_e} dS \tag{2}$$

$$\underline{F} = \int_{S_1} \rho \underline{u}(\underline{u}\cdot\underline{n}_1) dS_1 + \int_{S_2} \rho \underline{u}(\underline{u}\cdot\underline{n}_2) dS_2 + \int_{S_1} p\underline{n}_1 dS_1 + \int_{S_2} p\underline{n}_2 dS_2 + \frac{\partial}{\partial t}\int_V \rho \underline{u} dV \tag{3}$$

2. CFD simulations

The results of a three-dimensional fully unsteady CFD simulation [14] were used to analyze the stall force characteristics. The tested rotor was an industrial impeller with high peripheral Mach number, for which unique experimental pressure measurements, including the spatial reconstruction of the pressure field at the diffuser inlet, were available from a former analysis [15]. The computational domain included the impeller, the vaneless diffuser and the return channel (Fig.1(b)). Simulations were carried out with the TRAF code [16]; the code is a steady/unsteady, multigrid/multiblock flow solver for the three-dimensional Reynolds-averaged Navier-Stokes equations. A detailed description of the numerical scheme can be found in [16]. The domain included all stage components between Sect. 10 and Sect. 60 in Fig.1(b). Experimental values were used to apply the boundary conditions at Sect. 10 (spanwise distributions of total pressure, total temperature, and flow angles), while at Sect. 60 the static pressure was imposed at the hub and its spanwise distribution was obtained using the radial equilibrium.

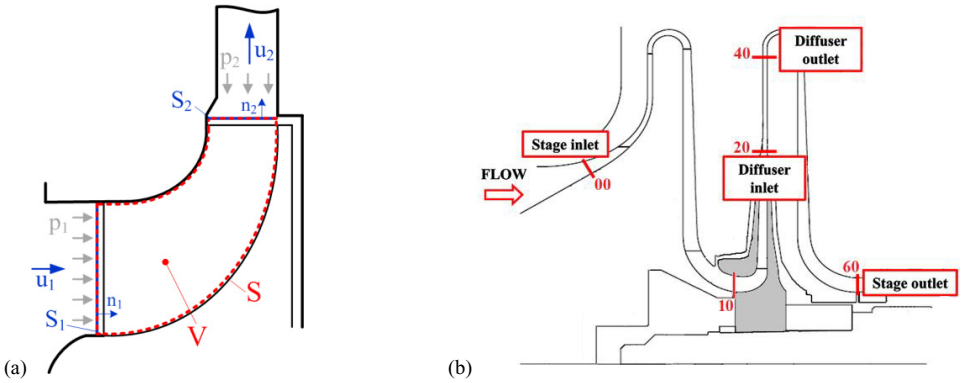

Fig. 1. (a) Control volume for the theoretical analysis of stall force; (b) Computational domain in CFD analyses [14].

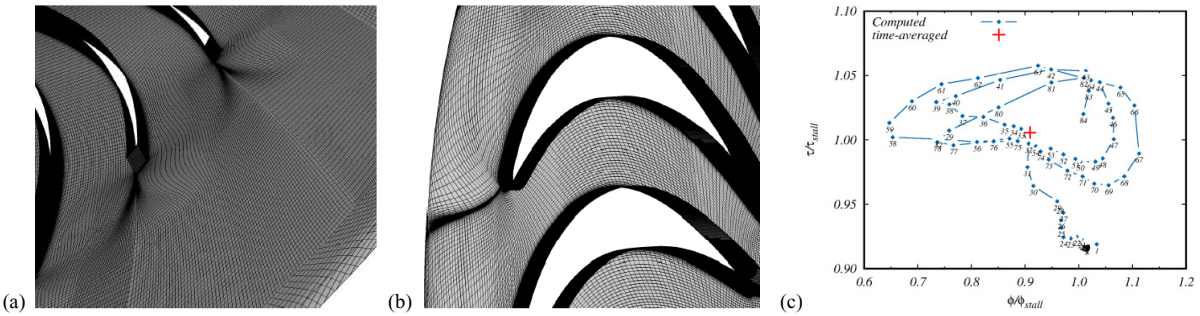

Fig. 2. Mesh details [14]: (a) impeller and vaneless diffuser (b) return channel. Normalized work and flow coefficients evolution (c).

The domain was discretized using structured grids (some detailed views are reported in Fig. 2(a) and Fig. 2(b)), obtained with in-house developed elliptic mesh generators. Non-periodic H-type grids for each blade passage were used. In particular, for the impeller passage and the vaneless diffuser a single-block H type grid was adopted for a total of 1.36M points. The interface between the vaneless diffuser and the return channel computational domains was positioned at Sect. 40 before the U-bend. For the return channel a grid with 1.15M points was used. The overall grid dimension was of approximately 55.5M points. The value of the y^+ for the first grid point above the wall surface was below 1 for all the blades, and a low value of the mesh stretch was adopted in order to achieve a good resolution in the wall adjacent region. The mesh was selected on the basis of previous analyses on centrifugal compressor stages (e.g. [17]) and represents a reasonable compromise for the full-annulus unsteady computations. The one-equation Spalart-Allmaras model [18] was used as turbulent closure, together with the modification proposed by Spalart and Shur [19] to account for rotation and streamline curvature effects. Beyond the reference study of [14], this model has been recently used by the authors for the analysis of a turbocharger stage with a vaned diffuser [20], demonstrating robustness and low computational requirements with respect to the two-equation turbulence models. For brevity reasons, other details on the numerical scheme used in the present simulations are not reported here; additional detailed information can be found in [14]. It is worth noticing, finally, that the comparison between experiments and simulations, also reported in [14], showed a really good matching and corroborated the CFD capabilities in correctly describing the phenomenon.

3. Results

Eighty-four full impeller revolutions were simulated with the unsteady approach. As discussed in [14], after about 10 periods of the simulation an instability developed, which substantially increased the amplitude of the lift fluctuations on the impeller blade. The evolution of the stage performance parameters, namely the work coefficient and the flow coefficient, is shown in Fig. 2(c). Performance parameters were calculated considering the time-averaged values of the mass-weighted total enthalpy and the work-averaged total pressure, and normalized with respect to the corresponding experimental values at stall inception [15]. The red cross in the figure represents the time-averaged value over 20 full revolutions which corresponds to a pseudo-periodicity of the rotating stall that has been already analyzed in [14]. In order to analyze the aerodynamic force connected to the onset of the rotating stall pattern, 20 relevant revolutions were here selected, namely between t/T=64 and t/T=84, where T represents the period of an impeller revolution. Figure 3 depicts the pressure evolution within the vaneless diffuser in the analyzed time window. Data are reported in terms of dimensionless pressure fluctuation p^* at Sect. 20 (diffuser inlet, where experimental probes were located), equal to the pressure fluctuation divided by the mean pressure at Sect. 20.

As discussed by the authors in [14], in the first part of simulations the flow structure was yet not fully coherent. The transition mode towards the final stall structure took place at approximately t/T=71, and led to a stable pattern for a few revolutions. The intensity and frequency of the predicted pattern were found to be in excellent agreement with the experiments presented in [15]; on this basis, present data are thought to be a valuable case study for a general-validity analysis of the force contributions. The subsynchronous frequency of the stall (approximately 5% of the revolution frequency) is clearly distinguishable in the map presented in Fig. 3.

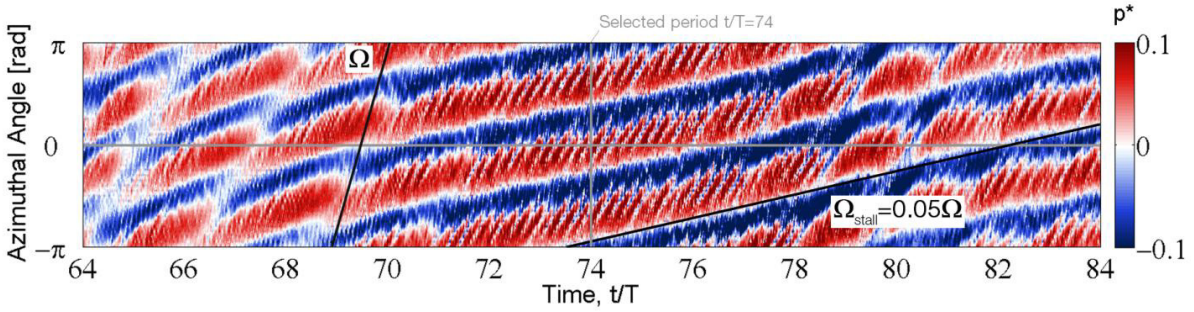

Fig. 3. Pressure evolution in the diffuser at Sect. 20 during 20 full revolutions (stall period).

In the present study, two different analyses were carried out, aimed at assessing two main assumptions that are made in the experimental procedure to evaluate the stall force, i.e. the possibility of neglecting the momentum contribution with respect to the pressure one (see Eq. 3) and the stability of the stall pattern during its revolution, which is pivotal to enable the shift between time and space domain made by the ensemble averaging process.

3.1. Analysis of force contributions

To analyze in details the different force contributions, the relevant revolutions between t/T=71 and t/T=76 were analyzed. In this time window, the stall pattern is indeed coherent and structured; for the same reasons, the same revolutions were also analyzed in [14] and compared to experiments. During the selected time window, the radial (destabilizing) force on the impeller was first directly calculated by CFD by integrating the contributions all over the impeller rotating surfaces. The calculated values are reported in Fig. 4(a) in a green line and denoted as F_r*, since they are reported in a dimensionless form (i.e. the force divided by the area at Sect. 20 and the mean pressure herein) to preserve the non-disclosure agreement with the industrial partner. In the same figure, the force calculated as the integral of pressure and momentum contributions at Sect. 20 is also reported in a red line. As theoretically attended, an excellent agreement was found between the two calculation methods. It is also worth noticing that several ripples are noticed in the force trend; these ripples indeed do not correspond to the main modulation induced by the rotating stall, as it will be shown later on. The force variability is conversely due to the additional phenomena taking place during the simulated stall conditions and discussed in details in [14].

In Fig. 4(b), the global radial force calculated as the integral at Sect. 20 was then decomposed into its two main contributions, i.e. the pressure and the momentum ones (Eq. 3). In doing so, it is worth remembering that the main assumption of the experimental method proposed in [10-12] is that the momentum contribution is small enough to calculate the force only based on the pressure contributions all over the flow passage area at Sect. 20 (Eq. 4).

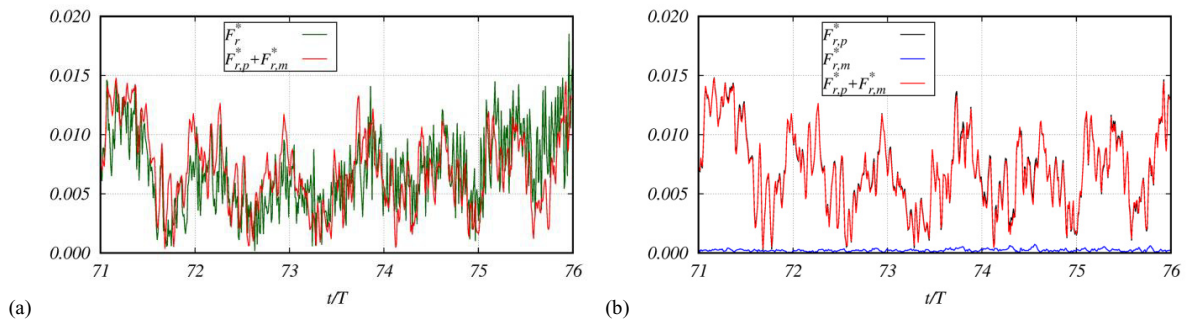

Fig. 4. Force on the impeller during the selected time window: (a) comparison between the radial force on the impeller directly calculated by the CFD and that obtained integrating the pressure and momentum contributions at Sect. 20; (b) magnitude of pressure and momentum contributions.

$$F = \int_0^{2\pi} p(\theta) b_{20} R_{20} d\theta \tag{4}$$

Present results soundly confirm the assumption of the experimental method, being the momentum contribution definitely negligible with respect to the pressure one. This indeed represents a very important result in view of future experimental studies on real machines, allowing the use of properly positioned dynamic pressure sensors only for the estimation of the stall force.

3.2. Time-space domain shift

The second main goal of the present analysis was to assess the suitability of the theoretical approach proposed in [10], which makes use of, at least, only two sensors for the reconstruction of the pressure field. Among the two, the signal of one sensor is in fact used to perform the ensemble averaging process, while the second one is used to calculate the phase shift and then assess the correct frequency to lock the average on.

In the present case, the stall frequency was known a priori from previous analyses [14]; as a result, the only virtual probe at θ=0 was considered for the analysis: the signal in time of this probe indeed corresponds to the horizontal grey line in Fig. 3. Then, the instantaneous spatial pressure profile at t/T=74 (vertical grey line in Fig. 3) was extracted from the CFD pressure map at Sect. 20.

If the assumptions of the method proposed in [10] are fulfilled, this spatial pressure profile should match the evolution of pressure seen in time by the fixed probe during a time period equal to that of the stall (i.e. approximately 20 times the revolution period T). To verify this hypothesis, in Fig. 5 the spatial pressure profile at t/T=74 (red line) is compared to the time data recorded by the virtual probe at θ=0 (light grey line). Based on the aforementioned assumptions, the time data were transposed in the space domain using the stall period (Eq. 5).

$$\theta = t \cdot \omega_{stall} = t \cdot \frac{2\pi}{T_{stall}} \tag{5}$$

Moreover, in Fig. 5 the same time signal was also reported after a low-pass filtering has been applied to it, locked at the impeller revolution frequency. The smoothing of this filter on the signal is indeed comparable to that obtained by averaging experimental data on many revolutions with the ensemble average approach [12].

Upon examination of the figure, it is apparent that a very good matching was obtained, soundly confirming the possibility of relying only on the data of a single probe for the pressure pattern reconstruction in the vaneless diffuser in case of developed rotating stall conditions (another probe is needed for the stall frequency definition). In the present case, little discrepancies can only be seen at the boundaries of the selected time window only due to the instability of the pressure pattern in those periods that has been already extensively discussed in analyzing Fig. 3.

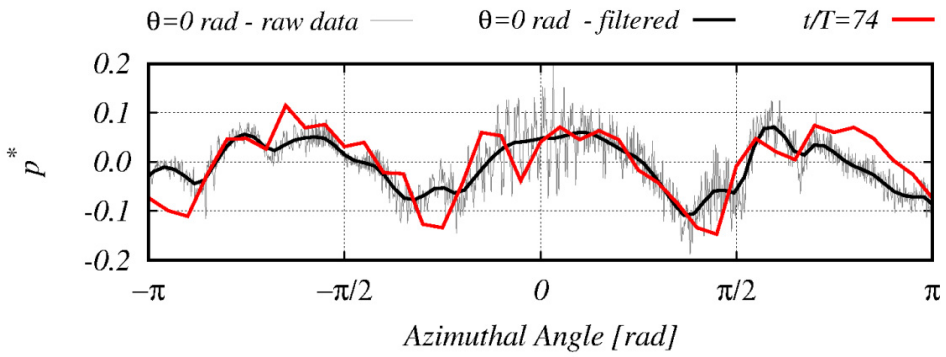

Fig. 5. Spatial pressure profile at Sect. 20 and t/T=74 compared to the time-dependent pressure data measured by the virtual probe at θ=0 transposed in space by the stall frequency as in the experimental approach based on the ensemble average.

In terms of stall intensity, both methods confirm an almost null value, due to the almost complete symmetry of the lobes: the result is again in agreement with experiments of [15]. An interesting assessment of the same considerations can be also obtained by analyzing the entire diffuser pressure maps during a stall cycle, reported in Fig. 6 for the mid span plane (the rotation of both the impeller and the stall lobe is counterclockwise). Please note that in the figure the impeller inlet has been hidden with a gray circle to preserve the non-disclosure agreement with the industrial partner.

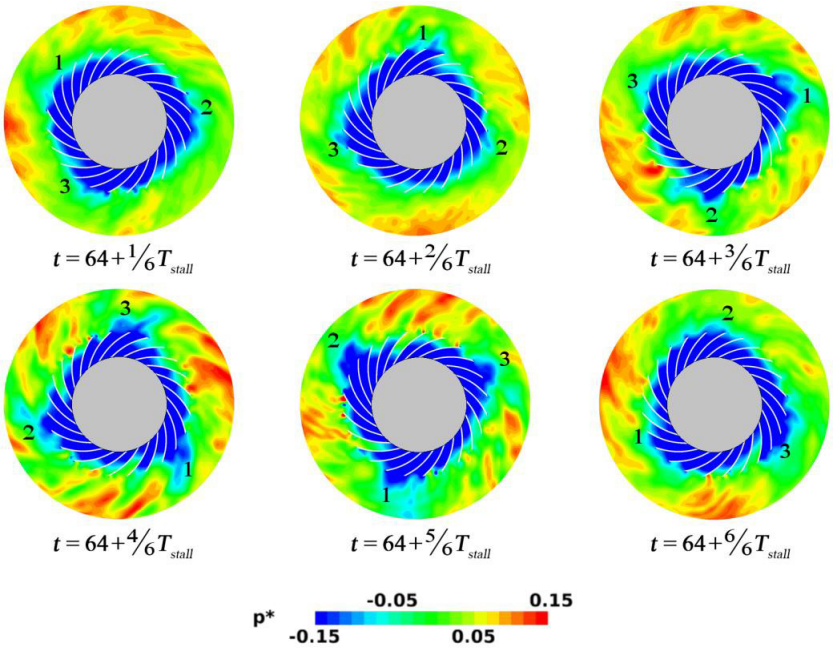

Fig. 6. Evolution of the pressure pattern within the diffuser (mid span) between t/T=64 and t/T=84.

Upon examination of the contours, acquired in correspondence to time intervals equal to $1/6\,T_{stall}$, the three-lobes nature of the stall is apparent, with the only partial exception of the first periods due to the already discussed instabilities in the stall pattern. Lobes are moving almost rigidly by approximately π/3 between every snapshot.

Finally, Fig. 7 reports the spatial pressure distribution at Sect. 20 and t/T=74 in the spanwise direction. As already noticed in [14], stall cells are definitely full-span. This result further enhances the confidence in the theoretical approach used in experiments, since allows the use of only two probes at mid span for a reliable force estimation.

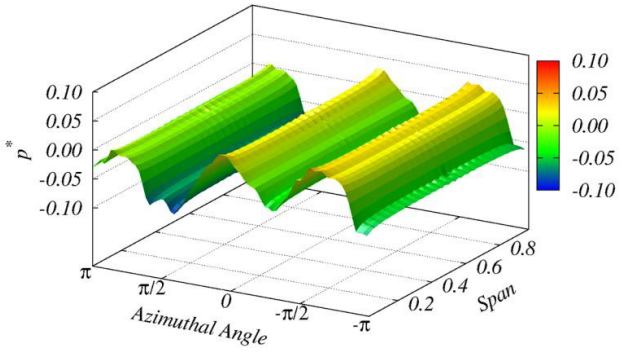

Fig. 7. Pressure distribution at diffuser inlet (Sect. 20) and t/T=74 as a function of circumferential and spanwise directions.

4. Conclusions

In the present study, fully unsteady three-dimensional CFD simulations of a centrifugal compressor stage under vaneless diffuser rotating stall conditions were exploited to analyze the characteristics of the resulting aerodynamic force on the impeller. In particular, the force value straightforwardly obtained by the CFD results was compared to that obtained by manipulating flow data at discrete points along the diffuser's inlet with the same theoretical approach that has been recently proposed for use in experimental tests.

The comparative analysis, whose results are indeed independent on the present case study and the specific stall pattern, showed that the shift of time-dependent data in discrete positions into the space domain using the ensemble average approach is an effective technique for the analysis of vaneless diffuser stall. Moreover, the stability of the developed stall pattern during its subsynchronous revolution allows the use of few sensors (at least two) for the reconstruction process with negligible accuracy errors. The full-span nature of stall cells also allows the instrumentation of a single spanwise section to achieve an accurate estimation of the force intensity. Finally, the present analysis also corroborated the main assumption of making use of pressure only for the estimation of stall force since the momentum contribution was proved to give negligible contribution to the final force intensity.

References

[1] Krain H. Review of Centrifugal Compressor's Application and Development. ASME J. Turbomach. 2005;127(1):25-34.
[2] Evans BF, Smalley AJ. Subsynchronous Vibrations in a High Pressure Centrifugal Compressor: a case History. Southwest Research Institute, San Antonio, Texas, NASA Tech. Rep., 1984.
[3] Sorokes JM, Marshall DF. A review of aerodynamically induced forces acting on centrifugal compressors, and resulting vibration characteristics of rotors. Proc. of the 29th Turbomachinery Symposium, Houston, Texas (USA), September 18-21, 2000, pp. 263-280.
[4] Ferrara G, Ferrari L, Mengoni CP, De Lucia M, Baldassarre L. Experimental investigation and characterization of the rotating stall in a high pressure centrifugal compressor: Part I: Influence of diffuser geometry on stall inception. ASME Paper GT-2002-30389. Proc. of the ASME Turbo Expo 2002, Amsterdam, The Netherlands, June 3-6, 2002.
[5] Ferrara G, Ferrari L, Mengoni CP, De Lucia M, Baldassarre L. Experimental investigation and characterization of the rotating stall in a high pressure centrifugal compressor: Part II: Influence of diffuser geometry on stage performance," ASME Paper GT-2002-30390, Proc. of the ASME Turbo Expo 2002, Amsterdam, The Netherlands, June 3-6, 2002.
[6] Cellai A, Ferrara G, Ferrari L, Mengoni CP, Baldassarre L. Experimental investigation and characterization of the rotating stall in a high pressure centrifugal compressor. Part III: Influence of diffuser geometry on stall inception and performance (2nd impeller tested). Proc. of the ASME Turbo Expo 2003, Atlanta, USA, June 16-19, 2003.
[7] Cellai A, Ferrara G, Ferrari L, Mengoni CP, Baldassarre L. Experimental investigation and characterization of the rotating stall in a high pressure centrifugal compressor. Part IV: Impeller influence on diffuser stability," Proc. of the ASME Turbo Expo 2003, Atlanta, USA, June 16-19, 2003.
[8] Ferrara G, Ferrari L, Baldassarre L. Experimental investigation and characterization of vaneless diffuser rotating stall. Part V: Influence of diffuser geometry on stall inception and performance (3rd impeller tested). Proc. of the ASME Turbo Expo 2006, Barcelona, Spain, May 8-11, 2006.
[9] Carnevale EA, Ferrara G, Ferrari L, Baldassarre L. Experimental investigation and characterization of vaneless diffuser rotating stall. Part VI: Reduction of three impeller results. Proc. of the ASME Turbo Expo 2006, Barcelona, Spain, May 8-11, 2006.
[10] Bianchini A, Biliotti D, Ferrara G, Ferrari L, Belardini E, Giachi M, Tapinassi L, Vannini G. A systematic approach to estimate the impact of the aerodynamic force induced by rotating stall in a vaneless diffuser on the rotordynamic behavior of centrifugal compressors. ASME J. Eng. Gas Turbines Power 2013;135(11):1-9.
[11] Biliotti D, Bianchini A, Ferrara G, Ferrari L, Belardini E, Giachi M, Tapinassi L, Vannini G. Analysis of the rotordynamic response of a centrifugal compressor subject to aerodynamic loads due to rotating stall. ASME J. Turbomach. 2015;137(2):1-8.
[12] Bianchini A, Biliotti D, Ferrara G, Ferrari L, Belardini E, Giachi M, Tapinassi L. Some guidelines for the experimental characterization of vaneless diffuser rotating stall in stages of industrial centrifugal compressors. Proc. of the ASME Turbo Expo 2014, Düsseldorf, Germany, June 16-20, 2014.
[13] Ferrara G, Ferrari L, Baldassarre L. Rotating Stall in Centrifugal Compressor Vaneless Diffuser: Experimental Analysis of Geometrical Parameters Influence on Phenomenon Evolution. Journal of Rotating Machinery 2004;10(6):433–442.
[14] Marconcini M, Bianchini A, Checcucci M, Biliotti D, Rubino DT, Ferrari L, Arnone A, Ferrara G. A Three-Dimensional Time-Accurate Computational Fluid Dynamics Simulation of the Flow Field Inside a Vaneless Diffuser During Rotating Stall Conditions. ASME J. Turbomach., doi: 10.1115/1.4034633, 2016.
[15] Bianchini A, Biliotti D, Rubino DT, Ferrari L, Ferrara G. Experimental Analysis of the Pressure Field Inside a Vaneless Diffuser From Rotating Stall Inception to Surge. ASME J. Turbomach. 2015;137(11):111007-1-10.
[16] Arnone A. Viscous Analysis of Three–Dimensional Rotor Flow Using a Multigrid Method. ASME J. Turbomach. 1994;116(3): 435–445.
[17] Marconcini M, Rubechini F, Arnone A, Ibaraki S. Numerical Investigation of a Transonic Centrifugal Compressor. ASME J. Turbomach. 2008;130(1):011010.
[18] Spalart P R, Allmaras SR. A One–equation Turbulence Model for Aerodynamic Flows. La Recherché Aerospatiale 1994;1:pp. 5–21.
[19] Spalart PR, Shur M. On the Sensitization of Turbulence Models to Rotation and Curvature. Aerosp. Sci. Technol. 1997;1(5):297–302.
[20] Rubechini F, Marconcini M, Arnone A, Scotti Del Greco A, Biagi R. Special Challenges in the Computational Fluid Dynamics Modeling of Transonic Turbo-Expanders. ASME J. Eng. Gas Turbines Power 2013;135(10):102701.